Characterization of photorefractive BCT:Rh crystals at 1.06μm by two wave mixing

A. Radoua, Philippe Delaye, R. Pankrath, Gérald Roosen

Characterization of the photorefractive BCT:Rh crystals at 1.06 µm by two-wave mixing

A. Radoua[(1)], P. Delaye[(1)], R. Pankrath[(2)], G. Roosen[(1)]

[(1)] Laboratoire Charles Fabry de l'Institut d'Optique, du Centre National de la Recherche Scientifique et de l'Université Paris-Sud, Bat. 503, Centre Scientifique d'Orsay, 91403 Orsay Cedex, France.

[(2)] Universität Osnabrück, FachBereich Physik, D 49069 Osnabrück, Germany

Abstract: We present an experimental investigation of the photorefractive properties of rhodium-doped barium calcium titanate (BCT) crystals of the congruent melting composition $Ba_{0.77}Ca_{0.23}TiO_3$. Considering the results previously obtained on these crystals in the visible region and at 850 nm wavelength, it should be a good alternative to $BaTiO_3$:Rh. Besides, the rhodium doping has the effect of making this material sensitive until the wavelength of 1.06 µm, a very technologically significant wavelength, because of the existence of the laser of strong power. Therefore we present here a study of rhodium-doped BCT crystals at 1.06 µm. These crystals are characterized by two wave mixing experiments. Two beam coupling gain factors up to 7.5 cm^{-1} with ordinary polarization and response time of the order of 1s, at incident power of 10 $W.cm^{-2}$, have been obtained. All the properties are explained with a three-center charge transport model, with the existence of iron impurity, which masks the influence of a rhodium at low doping concentrations.

PACS : 42.65 Hw, 77.84 S

Corresponding author : **P. Delaye**
Laboratoire Charles Fabry de l'Institut d'Optique, du Centre National de la Recherche Scientifique et de l'Université Paris-Sud, Bat. 503, Centre Scientifique d'Orsay, 91403 Orsay Cedex, France.
Tel : 33 1 69 35 87 50, Fax : 33 1 69 35 87 00, Email : Philippe.delaye@iota.u-psud.fr

I. Introduction

Barium titanate is one of the most employed photorefractive materials. Its remarkable performances make it an indispensable crystal for numerous applications such as phase conjugation or dynamic intracavity holography. These applications approach now more and more an industrial development. Unfortunately, the $BaTiO_3$ possesses a phase transition near 5 °C, which induces a loss of its photorefractive properties and can even destroy it. To remedy this problem, Osnabrück's university suggested, some years ago, and realizes the growth of a crystal derived from $BaTiO_3$, the $Ba_{0,77}Ca_{0,23}TiO_3$ (BCT) crystal in which this phase transition is thrown back below -100 °C [1]. This crystal is ferroelectric at room temperature and possesses the same symmetry group as $BaTiO_3$ (point group 4mm). The tensor of the electro-optic coefficients has thus the same structure as the one of barium titanate. The first results concerning this new crystal show that it has electro-optic coefficients of large values and high photorefractive gains in the visible region [2-7] that are comparable to what was measured in $BaTiO_3$.

$BaTiO_3$ is made sensitive in the infrared through rhodium doping. It has large self-pumped phase conjugated reflectivities and high two-beam coupling gains in this wavelength range [8 - 10]. This is of special interest for many applications, for example, self-pumped phase conjugation in advanced laser systems [11, 12] or laser-beam cleanup via two-wave mixing [13]. The infrared sensitivity is caused by Rh^{3+} and Rh^{4+}, which absorb light with wide absorption bands centered at the wavelengths 650 nm and 780 nm, respectively [14, 15].

The experiments made on rhodium-doped BCT crystals at 850 nm [16], showed that it is sensitive in the infrared region. As the absorption bands extends until the technology significant wavelength of 1.06 µm, BCT:Rh should also be sensitive at this wavelength where laser sources of strong power exist.

The ability for rhodium-doped BCT to be a real alternative to $BaTiO_3$:Rh depends on the properties of this new material. The goal of this study is to make the characterization of the photorefractive properties of the rhodium-doped barium calcium titanate (BCT) crystals at 1.06 µm. These characterizations are made thanks to measurements of the variation of the photorefractive performances according to parameters such as the grating wave vector or the incident optical power. The results are then compared with those predicted by the three-level charge transport model, two levels of rhodium ($Rh^{3+/4+}$, $Rh^{4+/5+}$) and one level of iron ($Fe^{3+/4+}$), model of the photorefractive effect already developed in the laboratory and validated by measurements at 850 nm.

II. Structure of the studied crystals

BCT crystal belongs to the octahedral of oxygen ferroelectrics family. It remains in the quadratic phase between -120 °C (at least) and 98 °C [1] and at ambient temperature, it has a spontaneous polarization directed along the crystallographic **c** axis, the symmetry of the crystal in this phase is 4mm. The tensor of the electro-optic coefficients at ambient temperature thus has the same form as that of barium titanate, i.e. it comprises 3 non zero electro-optic coefficients which are $r_{13} = r_{23}$, r_{33} and $r_{42} = r_{51}$. The first parameters measured on this crystal were the relative dielectric permittivities $\varepsilon_{11} = 1120$ and $\varepsilon_{33} = 240$ [1] and the electro-optic coefficients $r_{13} = 30$ pm.V^{-1} and $r_{33} = 130$ pm.V^{-1} [2].

We studied the BCT crystals doped with rhodium with quantities going from 100 to 10000 ppm added in the melt in order to understand the influence of doping on the photorefractive properties of the crystal at 1.06 μm. These crystals have a blue-green color. Their typical dimensions are 2×4×(4=c).

Figure 1 shows the absorption spectra of some of the studied crystals. We notice in this figure that the amplitude of the absorption band is proportional to the quantity of rhodium introduced into the crucible. It is also noted that the value of absorption stays very low for the wavelengths higher than 1 μm, with a maximum value of 0.11 cm^{-1} in the 10000 ppm doped sample.

III. Experimental set-up

III.1. Description of the experimental set-up

A two beam coupling characterization of a photorefractive crystals generally consists in a measurement of the variation of the photorefractive energy transfer gain as a function of the grating spacing and of the incident illumination, to which we can add a measure of the response time of the crystal as a function of these same parameters. These are the measurements we have performed, and we will now describe the experimental set-up and the procedure used to extract the gain from the energy transfer curves we acquire.

The main interest of the grating dependence of the gain is that it allows the determination of the effective trap density of the crystal through the determination of the position of the maximum of the dependence curve. To determine this maximum, it is now known [17] that it is better to perform two measurements; at low values of the grating spacing (i.e. with co-propagating beams) and,

beyond the maximum, at large values of the grating spacing (i.e. with counter-propagating beams). We thus implement two set-ups to allow both kind of measurement. They are shown in Fig. 2. The beam of a Nd:YAG laser, emitting at 1.06µm (two lasers with a power of 600 mW and 2.5 W were used), is collimated and its power controlled by a half wave plate followed by a polarizer. It is splitted to form a signal and a pump beam that are sent to be incident on the same side (in the co-propagating geometry) or on opposite sides (in the counter-propagating) of the photorefractive crystal. In both geometries the grating vector is oriented along the c-axis of the crystal. The signal beam is attenuated compared to the pump beam in order to be in the undepleted pump approximation and to work with low grating modulation. After the crystal, the signal beam is sent on a detector after some spatial filtering that allows to eliminate the scattering of the pump beam on defects of the crystal.

Due to the low absorption of the crystals and thus their low photoconductity, we had to focus the beam to increase the power density of the beams. The signal beam is focused in the crystal to have a small dimension beam, and the pump beam is focused a little after the crystal, in order to have a small dimension beam, that stays nevertheless larger than the signal beam to have a good overlap of the signal beam. This overlapping is easy to realize in the counter-propagating geometry where beams cross with a small angle. It is more problematic in the co-propagating geometry as it prevents the use of large angle between the beams and thus limits the available range of grating spacing.

Another problem with the focusing is the relative uncertainty in the determination of the power density incident on the photorefractive crystal, linked to the difficulty in the determination of the diameter of the pump beam. To determine this incident density of power, we use a power-meter to measure the power of the pump beam (much higher than that of the signal beam) in front of the crystal. We measure then the distance covered by the laser beam before and after each lens until it arrived at the entrance face of the crystal. We know the focal length of each lens used and the characteristics of the laser (diameter, position of the waist, divergence and the parameter M^2 of the laser). They are the data necessary to calculate the propagation of the laser beam and the expected radius r of the incident beam on crystal, by using an usual ABCD software. The density of power dP is given by ($dP = P/S$), with P the power and S ($S = \pi r^2$) the surface of the laser beam at the entrance of the crystal. The uncertainty of the measure is due to the determination of the position of the crystal compared to the focal point of the lens. But the main uncertainty of this measure is the value of the parameter M^2 of the laser, in particular for the laser 600 mW for which we have only $M^2 < 1.5$, which involves an uncertainty of 50 % on the absolute value of illumination, according to

the value of M^2 used in this calculation. This uncertainty prevents us to compare directly the intensity variation of the gain or of the response time between different crystals and for different grating spacings for a given crystal. In the following, absolute values of the power density are given, but they are only an order of magnitude of the incident power. Only relative intensity measurements are reliable enough to allow extraction of the data.

This focusing of the beam allows us to work with a small interaction zone of the crystal that can be supposed uniform and allows to minimize to a certain extent the effect of the not very good optical quality of some of the samples, that present striations and sometimes domains (Fig. 3). This allows to performed reliable measurements in all the samples except in the 10000ppm crystal in the co-propagating geometry.

III.2. Measurement procedure

To make reliable measurements we use the following procedure (Fig. 4):

* we open the signal beam for a few seconds to measure its intensity
* then we tur-off the signal beam and we put the pump beam on for a few seconds to measure the intensity of the pump beam scattered by the crystal defects
* then we launch the signal beam and we measure the amplitude of the energy transfer after it reaches steady state.
* the signal beam is then switched off and we measure the erasing of the grating by the pump beam.

In some measurements, we notice a small decrease of signal after it reaches "steady-state". This problem has been attributed to some oscillation of the pump beam in the crystal [18] due to the large gain and low absorption that changes the illumination condition of the crystal during the measurement. To prevent this problem, we illuminate the crystal with the pump beam before each measurement for some minutes, in order for it to reach a steady state illumination condition. This precaution allows to obtain reliable measurement and stable energy transfer each time. Only remains some unpreventable spikes attributed to some vibrations of the set-up that move rapidly the illumination pattern in front of the slow index grating, destroying for a small instant the optimal condition for the energy transfer. Most of the time these spikes do not prevent the treatment of the curves.

The time evolution curves (Fig. 4) obtained with the described process allows to extract all the parameters we want to determine, i.e. the photorefractive gain and the response time, in several manners, that we will now describe.

III.3. Extraction of the gain and validation of the experimental process

To determine the photorefractive two wave mixing energy transfer gain we carry out two types of measurements, that should both give the same value of the photorefractive gain. On the one hand, we measure the attenuation (or the amplification) of the signal beam, which gives the photorefractive gain by the traditional expression:

$$\Gamma = \pm \frac{1}{d} \mathrm{Ln}\left(\frac{I_{s+p}}{I_s} \right) \qquad (1)$$

where I_s is the signal intensity without pump beam, I_{s+p} is the signal intensity with pump beam, d is the length of interaction of the two beams and the ± sign depends if we are in attenuation or in amplification regime (to compare directly gain data with opposite signs).

On the other hand, we measure the erasure of the grating and the reduction in the amplitude of the diffracted beam when the signal beam is turned-off. The advantage of the second measurement is that it does not result from inherent interference phenomena of the energy transfer (constructive or destructive interference of the transmitted signal beam and of the diffracted pump beam) and the curves obtained are thus more stable (fig. 4), because not disturbed by possible vibrations of the set-up. Unfortunately, this measurement is only possible for high gain for which the diffracted signal, that varies like $\left(1 - e^{\Gamma d/2}\right)^2$, is high enough. The diffraction gain is then given by relation [19]:

$$\Gamma_{diff} = \frac{2}{d} \mathrm{Ln}\left(1 \pm \sqrt{\frac{I_{diff} - I_d}{I_s}} \right) \qquad (2)$$

where I_d is the scattered pump intensity (supposed spatially incoherent), I_{diff} is the diffracted pump intensity just when the signal is turned-off, I_s is the signal intensity without pump beam and the ± signs depends if we are in the attenuation or in the amplification regime.

We can note here that we are in a pecular diffraction regime, that should be described by the two beam coupling model [19]. Indeed, we measure the diffraction of one of the writing beam. It is thus automatically at Bragg incidence, whatever its incidence and whatever its particular shape. This measurement is thus not disturbed by an eventual distortion of the wavefront induced by the defects of the crystal, that can be observed in a four wave mixing set-up [20].

From curves of kinetics of the photorefractive effect (Fig. 4), we obtain two measurements of the same phenomenon Γ and Γ_{diff}, which must thus give the same results, which is the case in general either in the amplification regime or in the attenuation regime (Fig. 5). This identity in both extraction of the gain, shows that the data obtained are really the expected photorefractive gain and

that no other phenomenon such as induced absorption or absorption grating disturbs the measurement. This last point is confirmed by the fact that the measured gain is the same in the amplification and in the attenuation regime at the precision of the measurement (Fig. 6). The induced absorption phenomena and absorption grating are thus negligible in BCT at 1.06 μm, compared to the usual values of the photorefractive gain.

From the temporal curves (Fig. 4), we can also measure the response time τ of the photorefractive crystal. As for the photorefractive gain we can extract it from the two kinetics curves at our disposition. For the energy transfer kinetics we can show [19] that, taking into account that the absorption of the crystal is very small and that the energy transfer gain stays moderate, the energy transfer establishment given by a simple exponential $e^{-t/\tau}$ variation giving directly the time constant of the crystal. For the erasure curve of the diffraction (that is preferred due to its better quality) the kinetics is adjusted by an exponential law of the form $e^{-2t/\tau}$.

IV. Dependence of the photorefractive parameters with grating spacing and incident illumination

We will now evaluate the evolution of the different measured photorefractive data as a function of the set-up parameters. First we will measure the variation of the space charge field as a function of the incident illumination, that will give us the minimum incident power density necessary to saturate the photorefractive gain. Then once verified that the incident power is sufficient to saturate the photorefractive gain we will measure its evolution as a function of the grating spacing for ordinary and extraordinary polarization. Finally we will determine the intensity evolution of the response time.

IV.1. Intensity dependence of the space charge field

The dependence of the photorefractive gain with the grating wave vector and the incidental intensity comes from the space charge field which is described in the majority of the cases by the general formula [21, 22]:

$$E_{sc}(k_r,I) = \frac{k_B T}{e}\eta(I)\frac{k_r}{1+\frac{k_r^2}{k_0^2(I)}} \qquad (3)$$

with the photorefractive gain given by:

$$\Gamma = \frac{2\pi}{\lambda_0} n^3 r^{eff} E_{sc}(k_r,I)(\hat{e}_s.\hat{e}_p) \qquad (4)$$

where $k_r = 4\pi n \sin\theta/\lambda_0$ is the grating wave vector, with θ the half-angle between the two beams inside the crystal. λ_0 is the wavelength, n is the refractive index, r^{eff} is the effective electro-optic coefficient, E_{sc} is the amplitude of the space charge field and $(\hat{e}_s.\hat{e}_p)$ the scalar product between the unit vectors parallel with the electric field of each beam. This scalar product $(\hat{e}_s.\hat{e}_p)$ depends only on polarization and takes values 1 or $\cos(2\theta)$ according to whether the light is ordinary or extraordinary polarized. In the performed experiments, we have $\cos(2\theta)\approx 1$ when co-propagating waves are used and $\cos(2\theta)=-1$ for counter-propagating waves, this term was thus simply taken into account by changing the sign of the measured counter-propagating gain (with extraordinary polarized beams) with respect to the co-propagating gain.

In the expression of the space charge field (3), $\eta(I)$ is given in a first approximation by the usual expression:

$$\eta(I) = \frac{1}{1 + \frac{I_{sat}}{I}} \tag{5}$$

that expresses the saturation of the gain with the intensity. It is connected physically to a competition between the thermal excitation and the optical excitation.

The second term dependent on the intensity in the equation (3) is the Debye wave number k_0 which is expressed as a function of the effective trap density N_{eff} as:

$$k_0^2(I) = \frac{e^2 N_{eff}(I)}{k_B T \varepsilon_0 \varepsilon^{eff}} \tag{6}$$

where ε^{eff} is the effective dielectric constant. The effective trap density informs us about the charge quantity available to take part for the photorefractive effect. It is made up of the involuntary impurities present in the crystal if it was not doped, and/or of the doping agents added at the time of growth. The dependence of this density with the intensity is due to a redistribution of the charge which can possibly take place between various photorefractive species. The importance of this intensity dependence is generally smaller and less direct than that of the thermal excitation. The experimental data are then adjusted with the expression

$$\Gamma(I) = \eta(I)\Gamma_\infty = \frac{\Gamma_\infty}{1 + \frac{I_{sat}}{I}} \tag{7}$$

with Γ_∞ that represents the gain at saturation, and I_{sat} the saturation intensity (i.e. the intensity for which the gain is divided by 2).

The experimental curves with the adjusted curves are shown in Fig. 7, for the different studied samples, and the parameters of the fit by equation (7) are shown in Table 1.

The results presented in Table 1 show a value of the saturation of the intensity of the order of 0.8 $W.cm^{-2}$, without a clear variation with the dopant concentration. This value is slightly higher than the value measured at the same wavelength in rhodium doped $BaTiO_3$ ($0.3W.cm^{-2}$ [18]) but keeps the same order of magnitude. This value is almost one order of magnitude higher than the one measured in the same samples at 850 nm [16], indicating a lower photoconductivity at 1.06 μm than at 850 nm (in proportion of the decrease of the absorption). The measurements also indicate that the saturation gain increases with this concentration indicating an increase of the effective trap density (as we use counter-propagating beams). This last point will be discussed in more detail later.

IV.2. Variation of the photorefractive gain as a function of the grating wave number

Measurements of the dependence of the photorefractive gain with the grating wave vector are traditional to determine the electro-optic coefficients and the effective trap density of a crystal. This measurement is performed at saturation with intensity and we study the dependence of the photorefractive gain with the grating wave vector while varying the angle between the two incident beams. The two beams have symmetrical angles of incidence compared to the normal with the input face, which means that the grating wave vector is parallel to the **c** axis.

Two types of measurements are carried out. On one hand, by using the set-up presented on Fig. 2a, we measure the gain with co-propagating beams, i.e. with a transmission grating. In this configuration, we carry out measurements for low values of the grating wave number (i.e. with $k_r^2 < k_0^2$). According to equation (3), we are in a situation where the gain is given by:

$$\Gamma = \frac{2\pi}{\lambda_0} n^3 r^{eff} \frac{k_B T}{e} k_r \qquad (8)$$

The linear dependence of the gain with the grating wave number enables us to determine the effective electro-optic coefficient. But it does not give us any information on the parameter k_0^2 and thus on N_{eff}, which corresponds in fact to a deviation from the linear dependence of the gain with the grating wave number for great values of this parameter. To determine k_0^2, we carry out another measurement with the configuration presented in Fig. 2b, which corresponds to a counter-propagating situation, that uses a reflection grating. We keep the same situation where the grating wave vector is parallel to the **c** axis but with an angle θ of π/2. In this configuration where the grating wave vector is very large (i.e. with $k_r^2 > k_0^2$), the gain is dominated by the term k_0^2 (see equation (3)). The addition of measurements in the co-propagating and counter-propagating configurations is enough to precisely determine the effective trap density [17], using an adjustment of the combined experimental data with the function:

$$\Gamma = Ar^{eff}(k_r)\frac{k_r}{1+\frac{k_r^2}{k_0^2}} \quad (9)$$

where $A = \frac{2\pi}{\lambda_0} n^3 \frac{k_B T}{e}$ is a constant which value is known. $r^{eff}(k_r)$ is the effective electro-optic coefficient that depends on the beam polarization. Its expression is given by (ordinary or extraordinary polarizations respectively):

$$r_o^{eff} = r_{13} \quad (10)$$

$$r_e^{eff} = r_{33}\cos^2(\theta) - r_{13}\sin^2(\theta) \quad (11)$$

with an angle dependence of r_e^{eff} that is taken into account and written as a function of the grating wave number. In the counter-propagating configuration, the beams propagate along the c-axis, and both polarization are in fact ordinary and then $\left|r_e^{eff}\right| = \left|r_o^{eff}\right| = r_{13}$). This expression used here is obtained neglecting the piezoelectric influence on the photorefractive effect. Taking into account this influence would change the exact expression of the electro-optic coefficient [23] (replacing r_{13} and r_{33} by more a more complex expression, still independent of θ) but not the shape of the curve as in all the experiments, the orientation of the grating vector stays parallel to the direction of the c-axis of the crystal.

Then, the dependence of the photorefractive gain with the grating pattern with ordinary polarization enables to obtain, by fitting with function (9), the two parameters r_{13} and k_0^2. By using these two parameters in the adjustment of the data obtained with extraordinary polarization, we obtain the value of r_{33}. The knowledge of k_0^2 allows the determination of the effective density N_{eff} using the relation (6) with $\varepsilon^{eff} = \varepsilon_{33}$ the relative dielectric constant, which intervenes in our configuration.

The measured data with the theoretical adjustment are presented in Fig. 8. The parameters obtained by the adjustment are presented in Table 2. Among the different samples, there is one exception, with the 10000 ppm doped sample in which no data for co-propagating beams could be obtained (as discussed previously). In order to nevertheless estimate the value of the effective trap density in this sample, we consider that the electro-optic coefficient of this crystal is known with a value equal to the average of the values measured in the other samples.

The average value of the r_{13} coefficient is around 30 pm.V^{-1}, whereas it is around 80 pm.V^{-1}, except for the smaller value of the second 1000 ppm doped sample, perhaps because of experimental problems due to the quality of the crystal. This value of r_{13} is higher than the one measured at 850 nm in the same samples [16], and shows a good accordance with the theoretical values of BCT, that give 34 pm.V^{-1} and 107 pm.V^{-1}, using here the values taking into account the

piezo-electric effect identifying r_{13} to $r_{22}^{eff}(0,0) = r_{13}^{S} + p_{13}^{E} e_{33} / C_{33}^{E}$ and r_{33} to $r_{33}^{eff}(0,0) = r_{33}^{S} + p_{33}^{E} e_{33} / C_{33}^{E}$ (see [23] for notations). Concerning the effective trap density, it is almost constant at low value of the doping concentration and increases above 2000 ppm doping concentration. Only the 100 ppm sample diverges from this evolution. We attributed this different behaviour to the fact that this sample was grown some years ago and that the concentration of compensating traps that assure charge equilibrium (and control effective trap density) may have change since then, due to change in growth conditions.

IV.3. Response time

The response time τ of a photorefractive crystal is an essential parameter when applications of a photorefractive crystal are considered. It depends on the grating wave vector and is primarily inversely proportional to the total incident illumination on the crystal. For technical reason discussed above (cf. § III.1), we were not able to have a measurement as a function of the grating wave number with the used set-up. We thus limit our measurement to the evolution of τ as a function of the power density of the pump beam (Fig. 9).

For the simplest model of the charge transport, the response time expresses as [24]:

$$\tau = \frac{\varepsilon\varepsilon_0 k_B T}{e^2} \frac{\kappa_p^2}{A_p \alpha_p I} \frac{1}{1 + \frac{k_r^2}{k_0^2}} \qquad (12)$$

where α_p is the absorption coefficient related to the mechanism of photo-excitation of the majority charge carriers (holes in the case of the BCT crystals), $\kappa_p^2 = (e/k_B T)\gamma_p N_0 / \mu_p$ is the square of the inverse of the diffusion length of the holes, γ_p is the recombination coefficient, μ_p is the mobility of the holes and the coefficient A_p is given by:

$$A_p = \frac{\beta_p + S_p I}{S_p I} \qquad (13)$$

where β_p is the thermal emission coefficient and S_p the photoionisation cross section of holes. For this model of charge transport, the response time is inversely proportional to the conductivity of the crystal, i.e. the sum of dark conductivity and photoconductivity. The latter is related to I and the former to thermal emission of charges. We thus made adjustment of the experimental data using the following general expression for the response time:

$$\frac{1}{\tau} = \frac{1}{\tau_d} + bI \qquad (14)$$

with τ_d the response time in the dark, b is a constant and I is the incident intensity. More complete expressions with non linear behaviour of photoconductivity (variation as a function of I^x) have also been used but they have not brought better adjustment, and have thus been abandonned.

The adjustments are correct and show the saturation of the response time at low power due to the dark time constant. The influence of this dark time constant is the same than for the intensity dependence of the photorefractive gain. We observe that the variation becomes linear ($\tau<\tau_d$) above 1 W.cm^{-2}, a value that corresponds to the one measured for I_{sat}. The parameters of the adjustment curves for the different samples are shown in Table 3. The dark time constant is of the order of 5 s in all the samples with no clear dependence as a function of the dopant concentration. The larger value of the 10000 ppm sample should be taken with some care. The longer time constants of this sample prevent to perform measurements at low intensity what decreases the accuracy in the determination of the dark time constant (Fig. 9). Due to the problems of calibration of the intensity the determined value of b is not reliable, for this experiment.

Concerning the absolute value of response time, we obtain response times smaller that 1s for all the samples at an incident power density of about 10 W.cm^{-2}. This value is quite rapid. It is of the same order of magnitude than the value found in Rh doped $BaTiO_3$ [12], if we take into account the different experimental conditions in the two measurements (different grating spacing, different doping, …).

IV.4. Discussion

The results obtained in BCT at the wavelength of 1.06µm are very similar to the ones previously published for the wavelength of 850 nm [16, 25, 26]. We measure an increase of the effective trap density with doping concentration above 2000ppm. Besides, we see a small tendency towards the decrease of the saturation intensity with increasing concentration, with absolute values, which are about one order of magnitude larger than at 850 nm. This last behaviour is linked to the lower absorption (and thus the lower photoconductivity) at 1.06 µm. We will now compare the experimental results with the theoretical curves calculated using the model developed to explain the photorefractive effect in BCT:Rh at 850 nm [16].

V. Charge transport in the BCT:Rh crystals

The modelization of the charge transport is essential to understand the phenomena responsible for the photorefractive effect in the crystal and to make the optimization of the growth

of the desired crystal. To make this modelization in the BCT:Rh crystals at 1.06 μm, we will use the charge transport model developed to explain the experimental results obtained at the wavelength of 850 nm [16], adapting the wavelength dependent parameters to the new wavelength.

V.1. Description of the model

The three-center charge transport model used to explain the photorefractive behaviour of BCT:Rh at 850nm, uses two levels of rhodium (Rh^{3+}/Rh^{4+} and Rh^{4+}/Rh^{5+} corresponding to the three charges states of this defect) and one level of iron (Fe^{3+}/Fe^{4+}) (Fig. 10), from which holes are generated.

Rh^{4+} and Fe^{4+} are the neutral states of the levels and we denote their concentrations respectively as N and N_F. Then Rh^{3+} and Fe^{3+} are regarded as recombination centers and Rh^{5+} as a generation center for holes, their densities are respectively noted N^-, N_F^- and N^+. The electrical neutrality of the crystal is achieved by shallow donor and acceptor densities N_d and N_a. The compensation density is denoted as $N_{ad} = N_a - N_d$. p is the density of the free holes. The photo-ionisation cross sections are denoted as S; β represents the thermal emission rates and γ the rates of recombination. Finally $N_T = N^- + N + N^+$ is the total density of rhodium and $N_{TF} = N_F^- + N_F$ is the total density of iron.

The charge transport equations [16] are simultaneously solved numerically in the steady state and we calculate the dependence of the photorefractive gain with the grating wave vector and the intensity of the pump beam in order to compare these calculated curves with the experimental results.

V.2. Initial set of parameters and numerical simulations

Among all the parameters that will influence the photorefractive gain, only the photoionizations cross-sections will vary with the wavelength. All the others parameters, should be the same at 1.06μm and at 850nm. We thus use as an initial set of parameters the one determined at that wavelength [16] (Table 4). The adjustment to the experimental data is then performed, by the only adjustment of the photoionization cross-sections of rhodium and iron. These cross sections may have an influence on the effective trap density through illumination dependent charge redistribution in the different levels. They will also influence the saturation intensity and more directly the absorption of the crystal. The approximations made here are the same than the ones done at 850nm, i.e. that the compensation density N_{ad} is regarded as a constant in all the crystals whatever the rhodium concentration. A departure from this assumption may explain the different

effective trap density observed in the 100ppm sample, as N_{ad} has a direct influence on this parameter, and knowing that this compensation may vary slightly with the growth condition especially in samples grown several years apart, such as the 100ppm sample compared to others samples. As for 850nm, the high saturation intensity is linked to the high value of the thermal ionization rate β_F, associated here with an even lower photoionization cross-sections of holes due to the larger wavelength.

The determined set of parameters is certainly not unique (such as the one obtained at 850nm from which it is derived). But the fact that a good accordance can be obtained, changing only the wavelength dependent parameters, confirms that this set of parameters is certainly not far from the real one. The obtained values for the absorption correspond to those measured (Table 5). The variation of the saturation intensity (Fig. 11) is more clear than the observed one but its amplitude is nevertheless smaller than one order of magnitude and stays comparable to the observed one if we take into account the rather limited accuracy of our measurement of these parameters.

Concerning, the grating spacing dependency, the effective electro-optic coefficient, is supposed to be a constant and the same in all the samples in the simulations. The experimental variation observed for the different samples was attributed to some phenomenon (crystal quality, depolarization, …) independent of the charge transport in the sample. We thus used for the adjustment of the experimental curves a value of the photorefractive gain normalized to the value of effective electro-optic coefficient determined by the adjustment. Then the only parameters that governs the variation with the grating wavenumber is the effective trap density. The results of the adjustments are shown in Fig. 12, and we have a reasonable accordance between the experimental data and the calculated curves (except for the 100 ppm sample as explained above). We see clearly that the rhodium doping concentration influences the effective trap density (and thus the gain in the counter-propagating regime) only above 2000 ppm. This behaviour is, as at 850 nm, due to the large concentration of residual iron that inserts in BCT during the growth [16].

VI. Conclusion

The sensitivity of rhodium doped BCT in the infrared makes this crystal a good alternative to $BaTiO_3$:Rh for applications that requires high photorefractive gain such as phase conjugation. We showed here that high gains and short response time can be obtained in this crystal at the wavelength of 1.06 µm. For example, we measure gains as high as 7.5 cm^{-1} with ordinary polarization, which means that the use of the higher r_{42} coefficient would lead to even higher

coefficients. Concerning the response time we measure values of the order of 1s for an incident power of the order of 10W.cm^{-2}. These performances confirms the interest of this crystal already shown by studies at 850nm.

The charge transport model used to explain the experimental results is the same than at 850nm, with two levels of rhodium corresponding to its three charge states ($Rh^{3+}/Rh^{4+}/Rh^{5+}$), and one level of iron (Fe^{3+}/Fe^{4+}). The experimental results also show that like at 850nm the influence of the residual iron doping is important and that better results may be expected if this iron can be eliminated. It is only above 2000ppm of rhodium added in the melt that rhodium becomes preponderant compared to iron. The main influence of iron deals with the high intensity required to saturate the gain, of the order of 1W.cm^{-2}, what might be a drawback for some applications using low power lasers.

Références

[1] C. Kuper, R. Pankrath, H. Hesse : Appl.Phys. A **65**, 301 (1997).

[2] C. Kuper, K. Buse, U. van Stevendaal, M. Weber, T. Leidlo, H. Hesse, E. Krätzig : Ferroelectrics **208**, 213 (1998).

[3] S. Bernhardt, Ph. Delaye, H. Veenhuis, D. Rytz, G. Roosen : Appl. Phys. B **70**, 789 (2000).

[4] H. Veenhuis, T. Börger, K., Peithmann, M. Flaspöhler, K. Buse, R. Pankrath, H. Hesse, E. Krätzig : Appl. Phys. B **70**, 797 (2000).

[5] M. Zgonik, P. Bernasconi, M. Duelli, R. Schlesser, P. Günter, M. H. Garrett, D. Rytz, Y. Zhu, X. Wu :Phys. Rev. B **50**, 5941 (1994).

[6] J. Neumann, M. Röwe, H. Veenhuis, R. Pankrath, E. Krätzig : Phys. Stat. Sol. (b) **215**, R9 (1999).

[7] H. Veenhuis, T. Börger, K. Buse, H. Hesse, E. Krätzig : J. Appl. Phys. **88** (2), 1042 (2000).

[8] G. W. Ross, P. Hribek, R. W. Eason, M. H. Garrett, D. Rytz : Opt. Commun. **101**, 60 (1993).

[9] B. A. Wechsler, M. B. Klein, C. C. Nelson, R. N. Schwartz : Opt. Lett. **19**, 536 (1994).

[10] M. Kasczmarek, R. W. Eason : Opt. Lett. **20**, 1850 (1995).

[11] A. Brignon, S.Sénac, J.-L. Ayral, J.-P. Huignard : Appl. Opt. **37**, 3990 (1998).

[12] N. Huot, J.M.C. Jonathan, G. Roosen, D. Rytz, J.Opt. Soc. Am. **B 15**, 1992 (1998).

[13] A. Brignon, J.-P. Huignard, M. H. Garret, I. Mnushkina : Appl. Opt. **36**, 7788 (1997).

[14] H. Kröse, E. Possenriede, R. Scharfschwerdt, T. Varnhorst, O. F. Schirmer, H. Hesse, C. Kuper : Opt. Mater. **4**, 153 (1995).

[15] N. Huot, J.M.C. Jonathan, G. Roosen, Appl. Phys. B **65**, 489 (1997).

[16] S. Bernhardt, H. Veenhuis, Ph. Delaye R. Pankrath, G. Roosen : Appl. Phys. B **72**, 667 (2001), (E) **74**, 287 (2002).

[17] Ph. Delaye, L. A. de Montmorillon, I. Biaggio, J. C. Launay, G. Roosen : Opt. Comm. **134**, 580 (1997).

[18] N. Huot, J.M.C. Jonathan, G. Pauliat, D. Rytz, G. Roosen, Optics Comm. **135**, 133 (1997).

[19] Ph. Delaye, L. A. de Montmorillon, G. Roosen : Opt. Comm. **118**, 154 (1995).

[20] U. Van Stevendaal, K.Buse, H. Malz, H. Veenhuis, E. Krätzig, J.Opt. Soc. Am. **B 15**, 2868 (1998).

[21] N. V. Kukhtarev, V. B. Markov, S. G. Odulov, M. S. Soskin, V. L. Vinetskii, Ferroelectrics **22**, 949 and 961 (1979).

[22] G. Montemezzani : Phys. Rev. A **62**, 053803 (2000).

[23] S. Bernhardt, L.Mize, Ph. Delaye, G. Roosen, J. Appl. Phys. **92**, 6139 (2002).

[24] K. Buse : Appl. Phys. B **64**, 273 (1997).

[25] S. Bernhardt, « Gyromètre à fibre à double conjugaison de phase : -étude d'un nouveau matériau photoréfractif ; -réalisation d'un démonstrateur », thèse de l'université de Paris XI, (2001).

[26] G. Roosen, S. Bernhardt, Ph. Delaye, 8th IUMRS International Conference on Electronic Materials (IUMRS- ICEM 2002) Xi'an (China), 10-14 Juin 2002, proceeding to be published in Optical Materials (2002).

Figure captions

Figure 1 : Absorption spectra as a function of wavelength for BCT:Rh crystals doped with different amounts of rhodium.

Figure 2 : Experimental setup for two-beam coupling experiments with copropagating (a) and counterpropagating waves.

Figure 3 : Image of the BCT:Rh (10000 ppm) crystal along the **a** axis and of the BCT:Rh (4000 ppm) crystal along the **c** axis by using a CCD camera.

Figure 4 : Attenuation of the signal beam by the energy transfer followed by the decrease of the diffracted pump beam when the signal is turned-off (see text for the explanation of the different terms).

Figure 5: Photorefractive gain measured in attenuation (a), and in amplification (b) as a function of intensity measured by two different techniques for a BCT crystal rhodium-doped 2000 ppm in the counterpropagating regime.

Figure 6: Photorefractive gain as a function of intensity measured in the two modes of attenuation and amplification for a BCT crystal rhodium-doped 2000 ppm in the counterpropagating regime.

Figure 7: Photorefractive gain as a function of intensity, in the counter-propagating geometry and in the attenuation orientation. The points correspond to experiments and the lines to the fitting curves.

Figure 8: Photorefractive gain as a function of the grating wave vector in ordinary (a) and extraordinary polarization (b). The points correspond to the experiments and the lines correspond to the fitting curves.

Figure 9: Dependence of the response time with the intensity, for the counter-propagating geometry. The points correspond to the experiments and the lines correspond to the fitting curves by using formula (14).

Figure 10 : Schematic energy level diagram of BCT:Rh crystal containing iron as an impurity.

Figure 11: Simulation of the dependence of the photorefractive gain with the intensity in ordinary polarization.

Figure 12 : Photorefractive gain according to the grating wave vector in ordinary polarization. The points correspond to the experiments and the curves to the simulation.

Table captions

Table 1 : Values of the saturation of intensities and the saturated gain for the BCT:Rh crystals.

Table 2: Values of the coefficients electro-optics and the effective trap density for the BCT:Rh crystals from 100 to 10000 ppm.

Table 3: Response time in the dark τ_d and the constant of proportionality of the reverse of the response time with the illumination of the BCT:Rh 1000 to 10000 ppm crystals.

Table 4 : Set of parameters found to fit the experimental results at 1.06 μm in the case of a three-level model compared with those at 850 nm. The wavelength dependent parameters that had been changed are indicated with bold characters. A typographical error gave a wrong value of β_F in [16], the correct value is taken here.

Table 5 : Absorption calculated theoretically and that measured in experiments crystals of BCT doped with rhodium to 1.06 μm.

Table 1 *: Values of the saturation of intensities and the saturated gain for the BCT:Rh crystals.*

Crystal	I_{sat} (mW/cm^2)	Γ_∞ (cm^{-1})
BCT:Rh (10000 ppm)	660	7.6
BCT:Rh (4000 ppm)	820	4.8
BCT:Rh (2000 ppm)	590	3.4
BCT:Rh (1000 ppm)(1)	770	3.4
BCT:Rh (1000 ppm)(2)	1130	2.6

***Table 2**: Values of the coefficients electro-optics and the effective trap density for the BCT:Rh crystals from 100 to 10000 ppm.*

Crystal	r_{13} ($pm.V^{-1}$)	r_{33} ($pm.V^{-1}$)	N_{eff} (cm^{-3})
BCT :Rh (10000 ppm)	30	82	26×10^{16}
BCT :Rh (4000 ppm)	30	84	13×10^{16}
BCT :Rh (2000 ppm)	33	81	7.1×10^{16}
BCT :Rh (1000 ppm)(1)	31	81	7.7×10^{16}
BCT :Rh (1000 ppm)(2)	23	74	8.1×10^{16}
BCT :Rh (100 ppm)	33	73	3.3×10^{16}

***Table 3**: Response time in the dark τ_d and the constant of proportionality of the reverse of the response time with the illumination of the BCT:Rh 1000 to 10000 ppm crystals.*

Crystal	τ_d (s)	b
BCT:Rh (10000 ppm)	28	0.10
BCT:Rh (4000 ppm)	2.6	0.22
BCT:Rh (2000 ppm)	5.8	0.19
BCT:Rh (1000 ppm)(1)	3.9	0.23
BCT:Rh (1000 ppm)(2)	6.1	0.19

Table 4 *:* Set of parameters found to fit the experimental results at 1.06 μm in the case of a three-level model compared with those at 850 nm. The wavelength dependent parameters that had been changed are indicated with bold characters. A typographical error gave a wrong value of β_F in [16], the correct value is taken here.

Parameters	Adjusted value for BCT :Rh at 1.06 μm	Adjusted value for BCT :Rh at 850 nm
Photo-ionization cross section of Rh^{5+} (m^2):S^+	$\mathbf{1{,}5\times10^{-22}}$	90×10^{-22}
Photo-ionization cross section of Rh^{4+} (m^2):S^-	$\mathbf{0{,}023\times10^{-22}}$	4×10^{-22}
Photo-ionization cross section of Rh^{4+} (m^2):S_F	$\mathbf{0{,}028\times10^{-24}}$	1×10^{-24}
Recombinaison rate of Rh^{4+} (m^3/s):γ^+	$2{,}92\times10^{14}$	$2{,}92\times10^{14}$
Recombinaison rate of Rh^{3+} (m^3/s):γ^-	$15\times\gamma^+$	$15\times\gamma^+$
Recombinaison rate of Fe^{3+} (m^3/s):γ_F	γ^+	γ^+
Thermal emission of Rh^{5+} (s^{-1}):β^+	2,3	2,3
Thermal emission of Rh^{4+}(s^{-1}) :β^-	1×10^{-4}	1×10^{-4}
Thermal emission of Fe^{4+} (s^{-1}):β_F	125×10^{-4}	125×10^{-4}
Total iron concentration (m^{-3}):N_F	64×10^{23}	64×10^{23}
Compensation density (m^{-3}):N_{ad}	$-0{,}82\times10^{23}$	$-0{,}82\times10^{23}$
Total concentration of rhodium for a 1000 ppm doped sample (m^{-3}):N_T	$3{,}3\times10^{23}$	$3{,}3\times10^{23}$

***Table 5** : Absorption calculated theoretically and that measured in experiments crystals of BCT doped with rhodium to 1.06 μm.*

Crystal	theoretical α (cm^{-1})	experimental α (cm^{-1})
BCT :Rh 10 000 ppm	0.128	0.108
BCT :Rh 4000 ppm	0.045	0.092
BCT :Rh 2000 ppm	0.021	0.023
BCT :Rh 1000 ppm	0.010	0.026
BCT :Rh 100 ppm	0.003	-

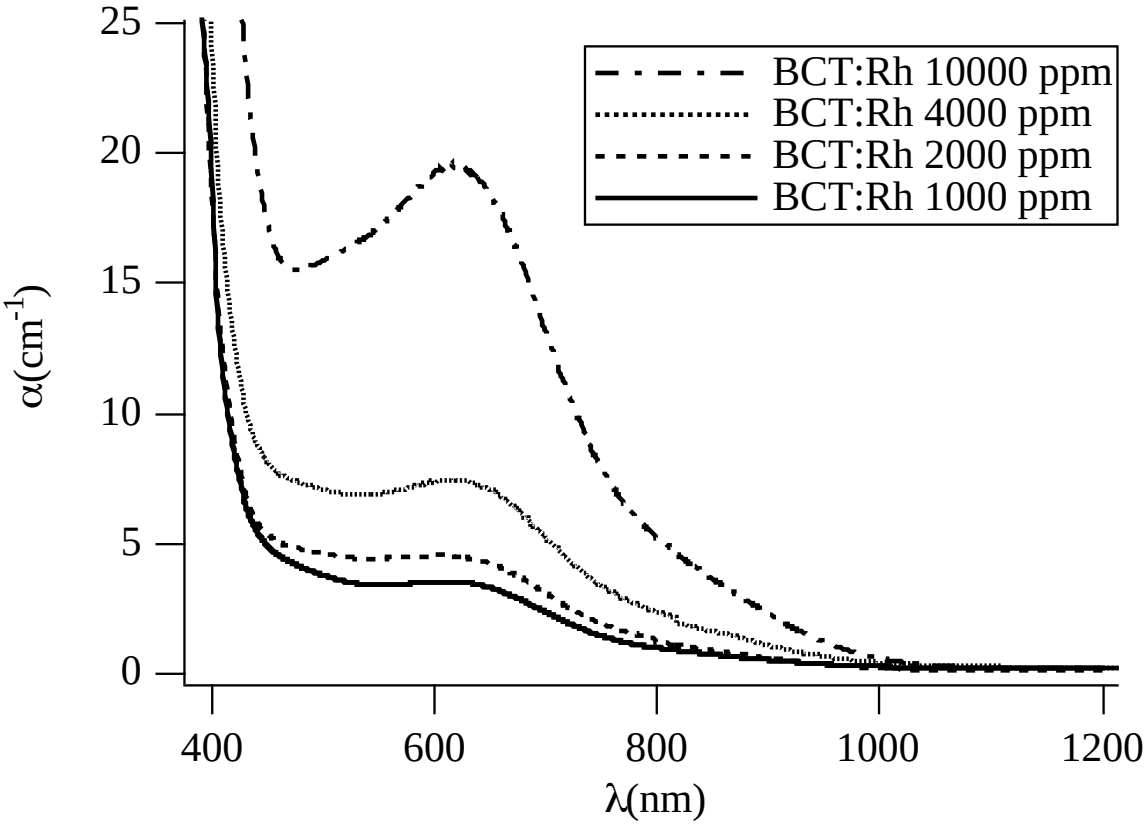

Figure 1 : A. Radoua et al.

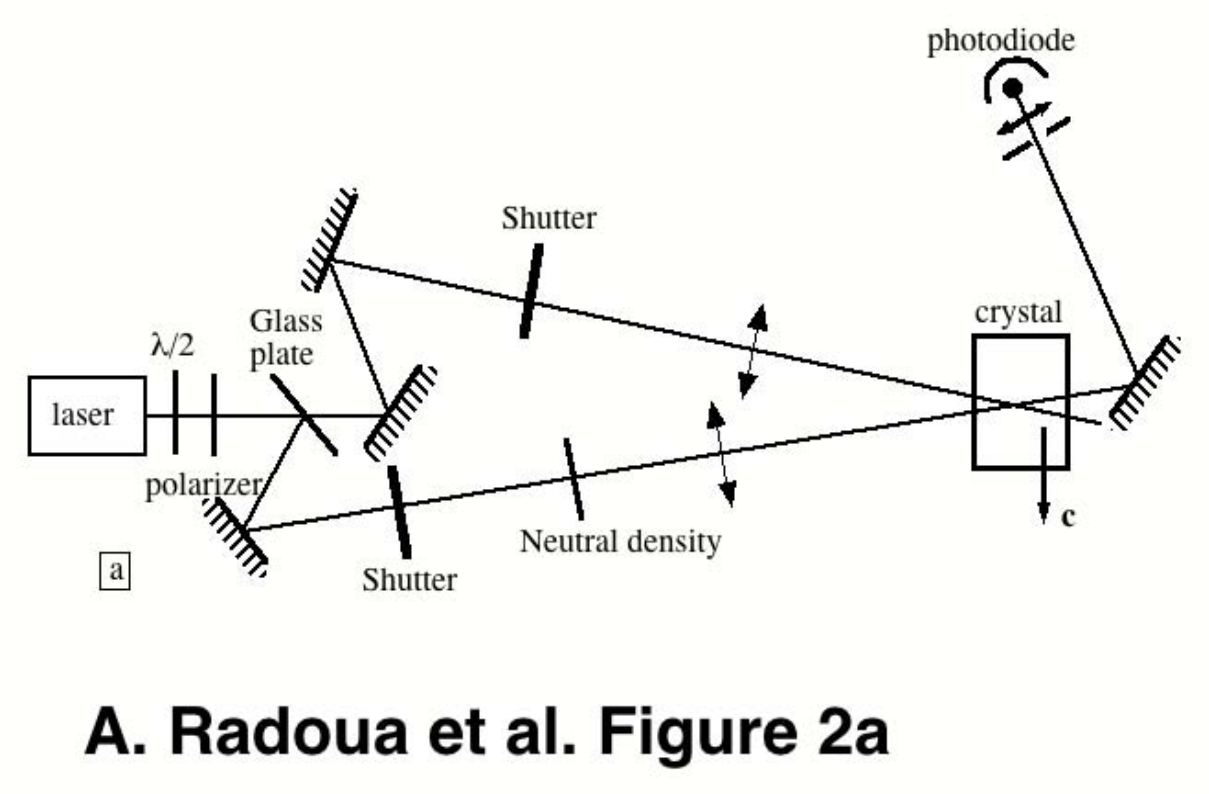

A. Radoua et al. Figure 2a

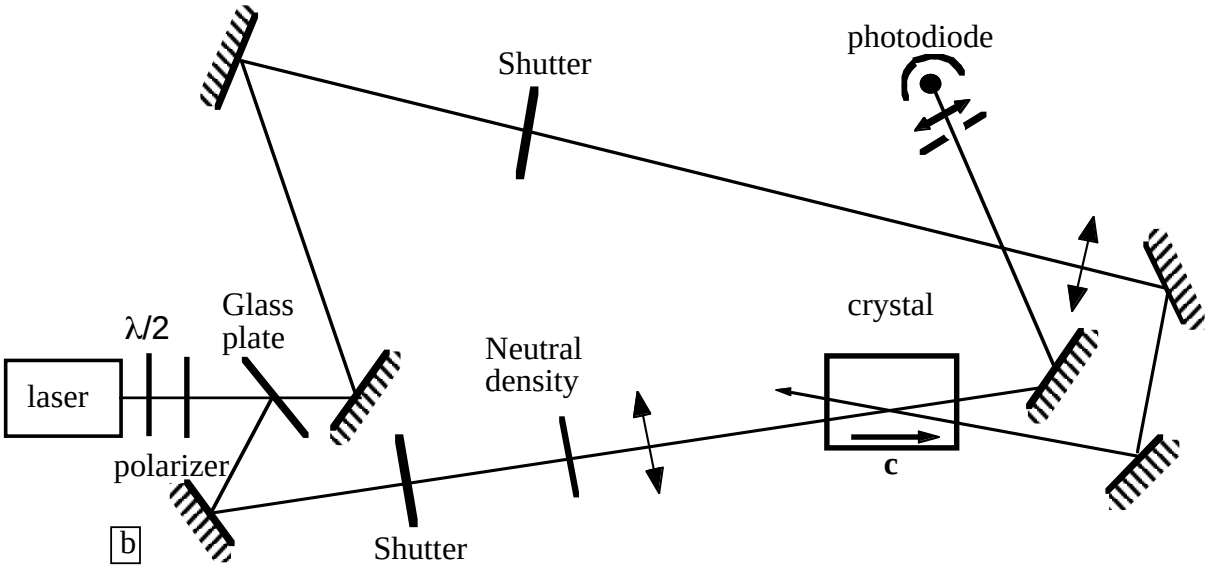

A. Radoua et al. Figure 2b

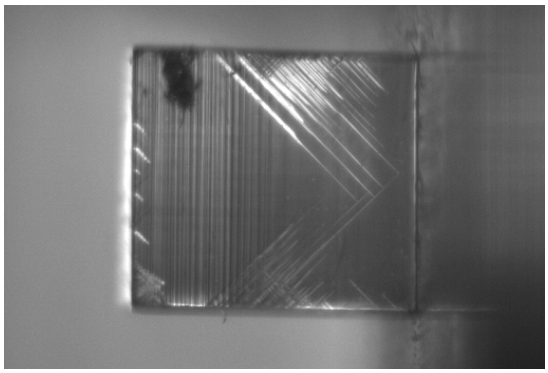

(a)

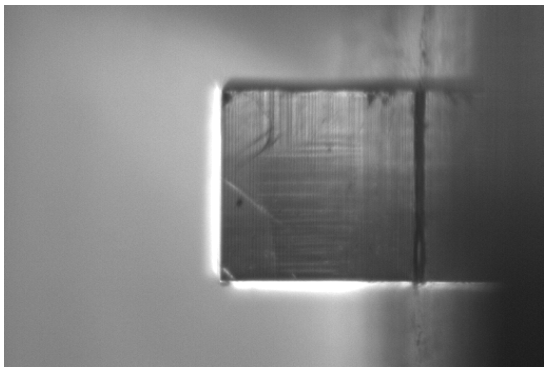

(b)

Figure 3 : A. Radoua et al.

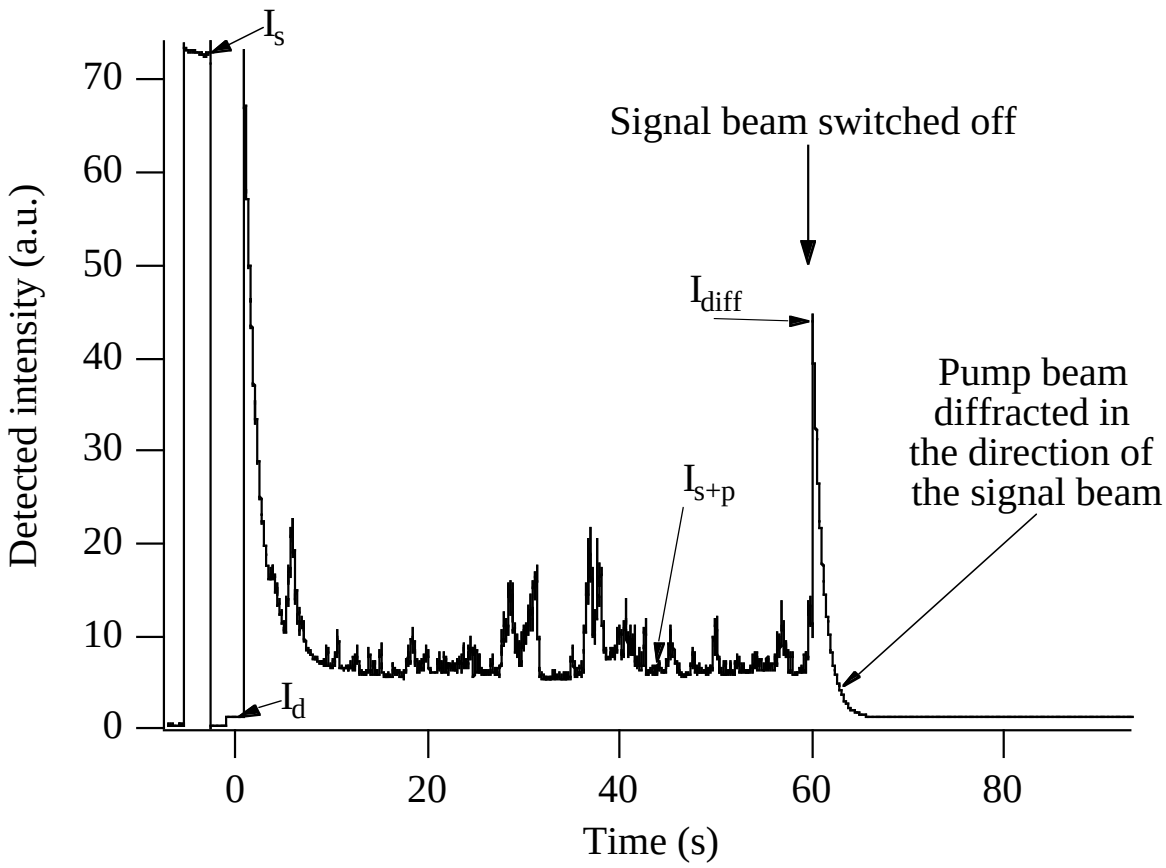

Figure 4 : A. Radoua et al.

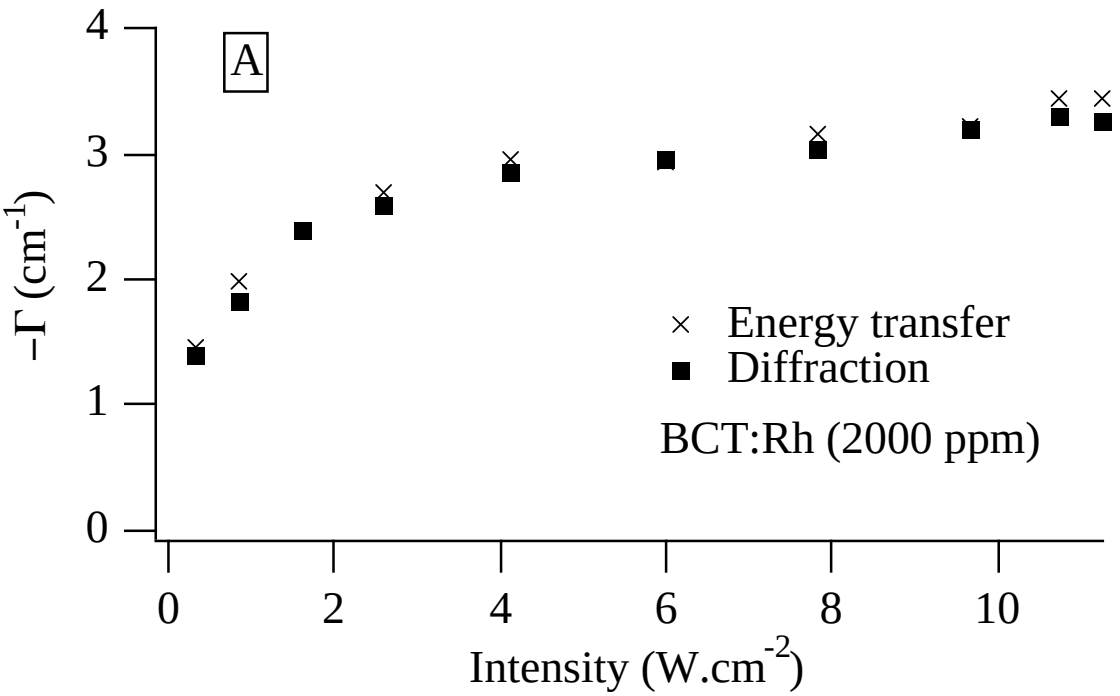

Figure 5A : A. Radoua et al.

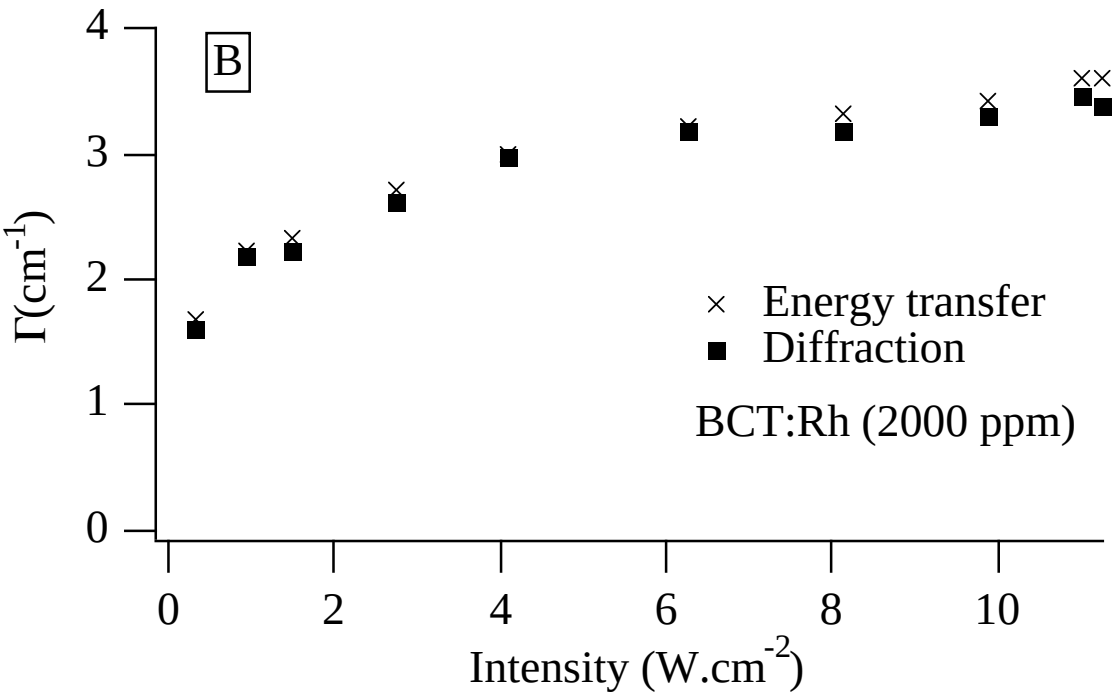

Figure 5B : A. Radoua et al.

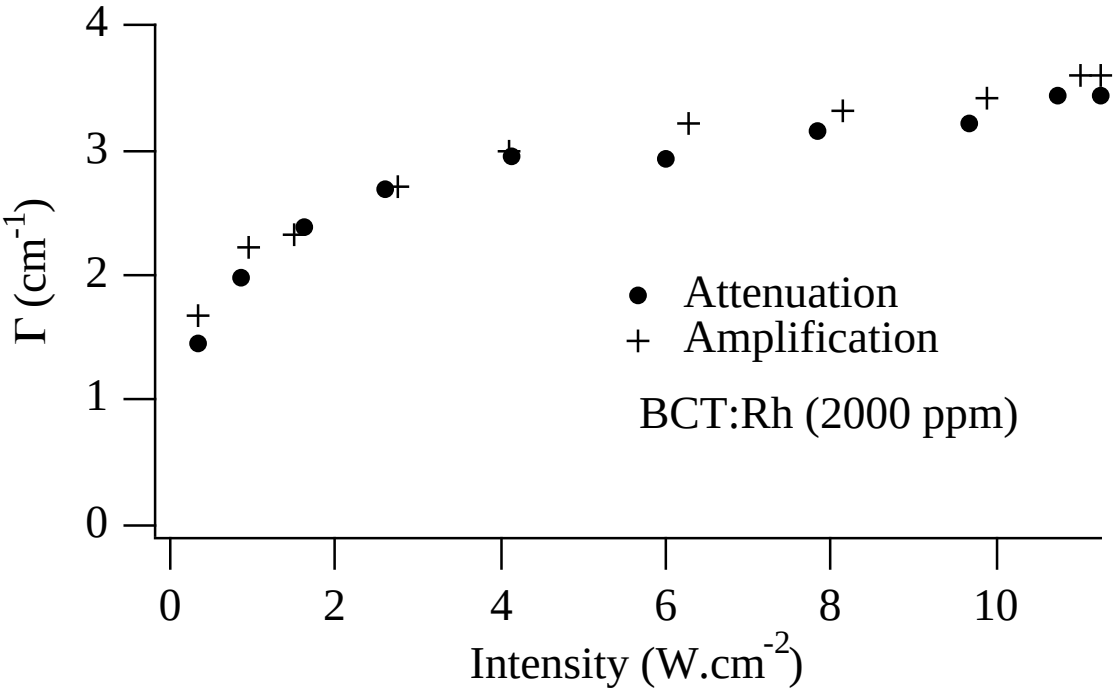

Figure 6 : A. Radoua et al.

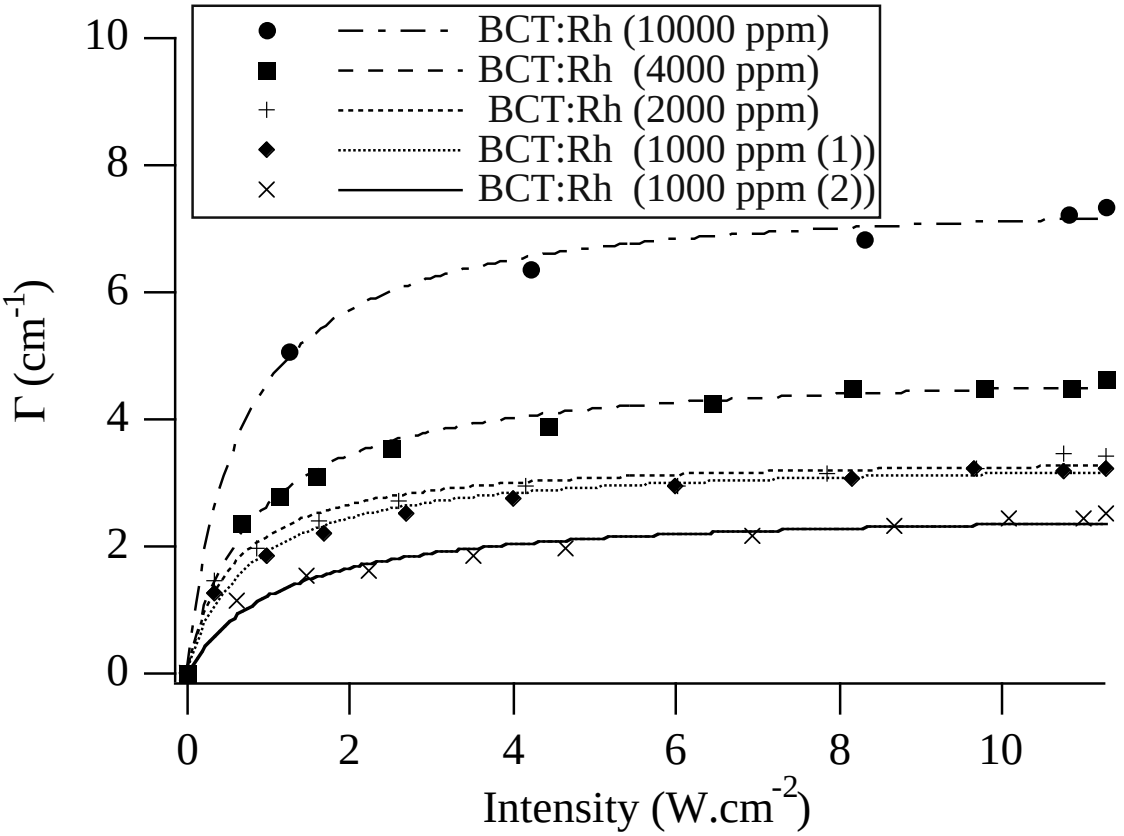

Figure 7 : A. Radoua et al.

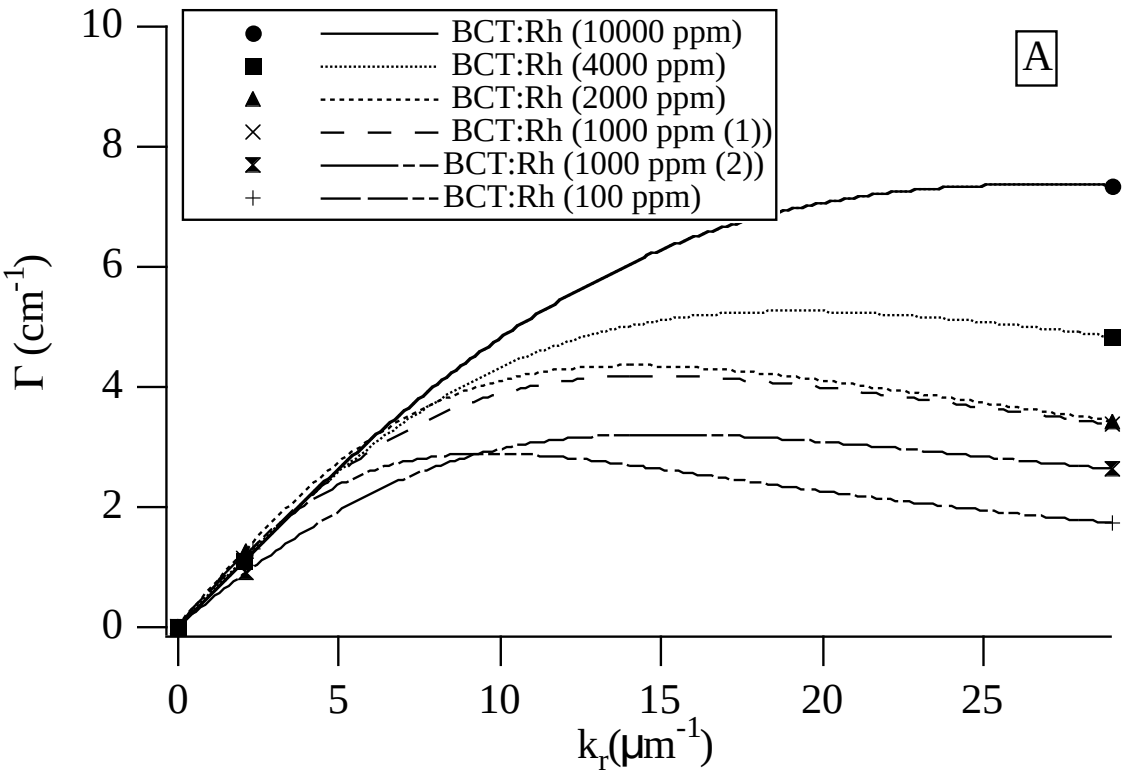

Figure 8A : A. Radoua et al.

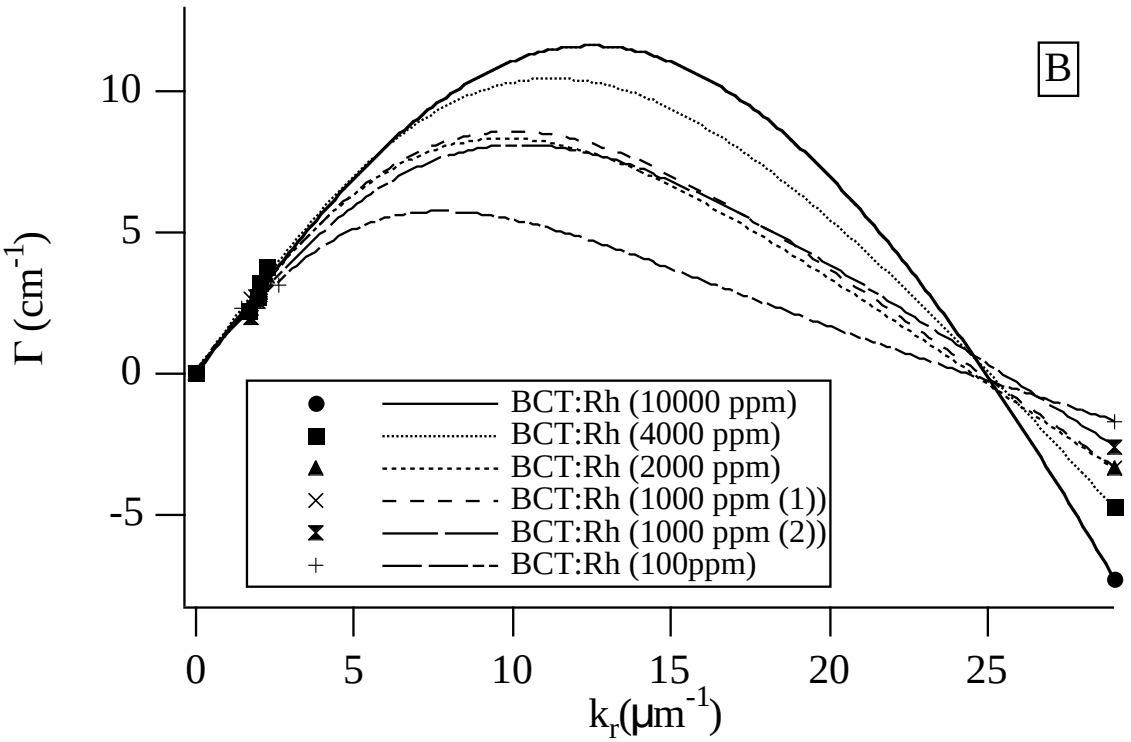

Figure 8B : A. Radoua et al.

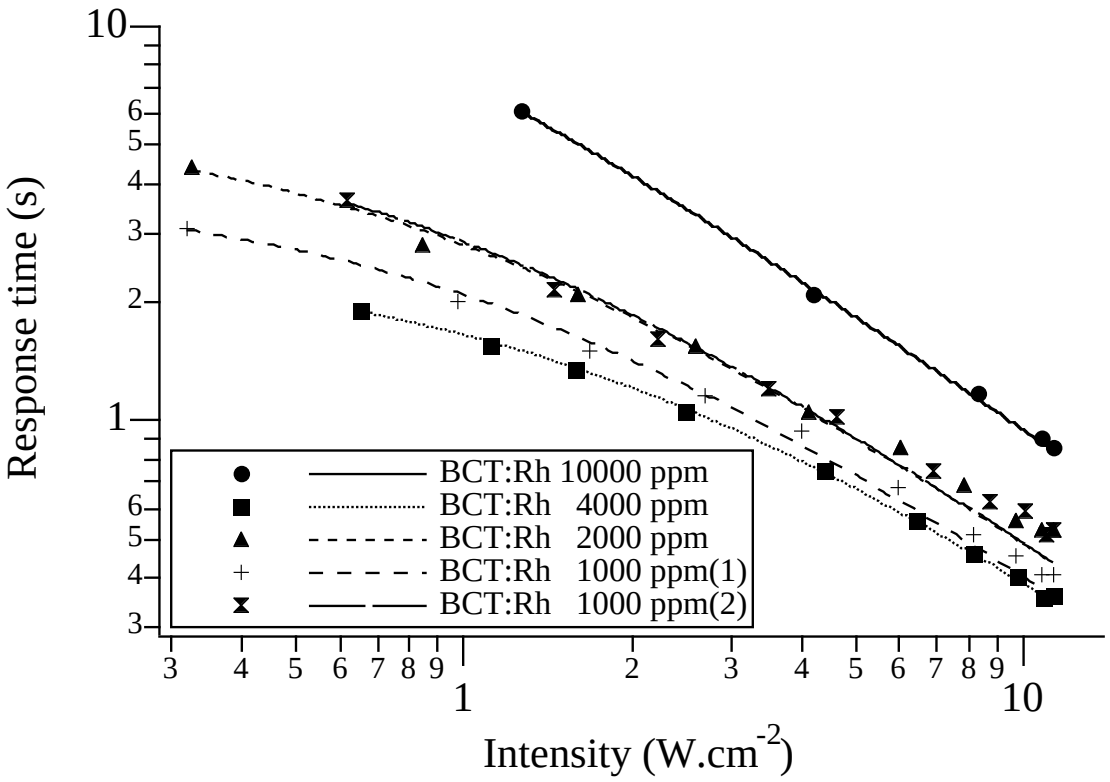

Figure 9 : A. Radoua et al.

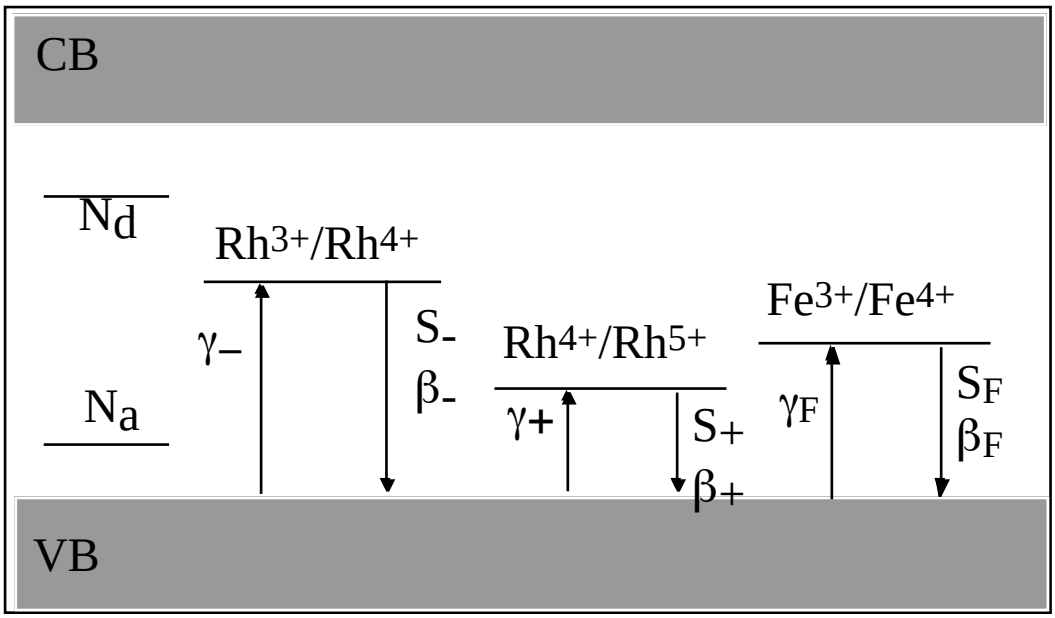

A. Radoua et al. Figure 10

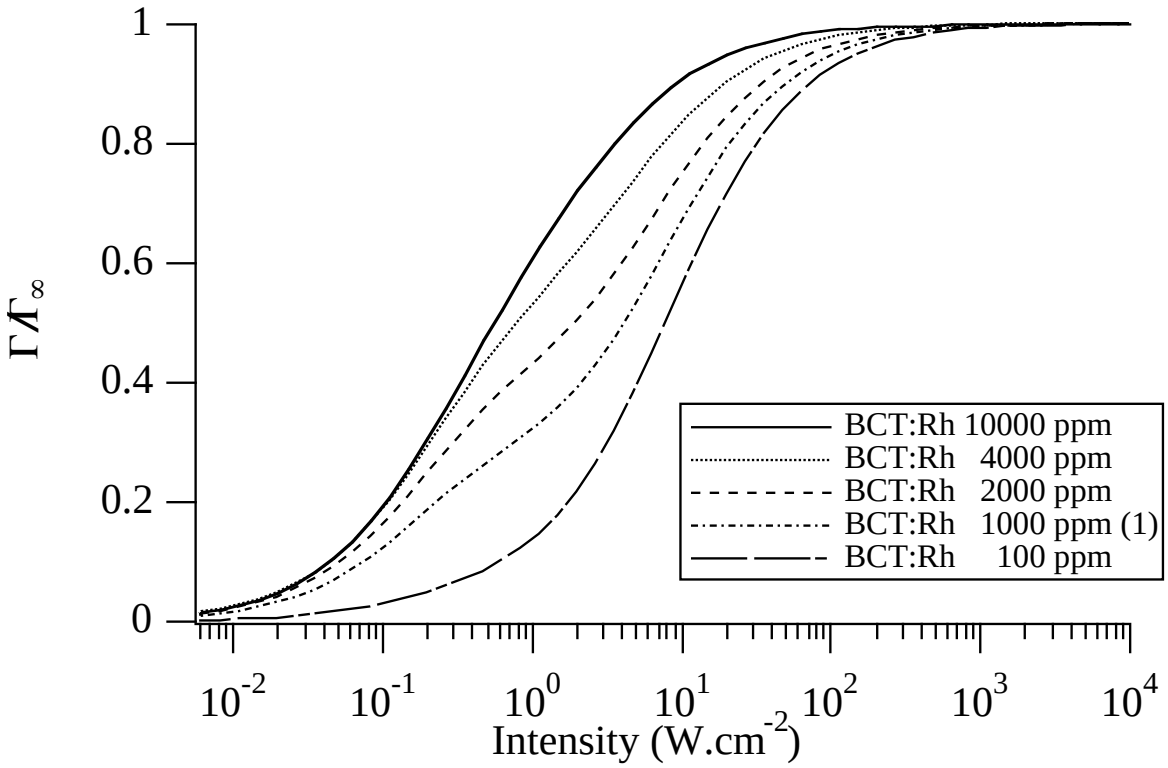

Figure 11 : A. Radoua et al.

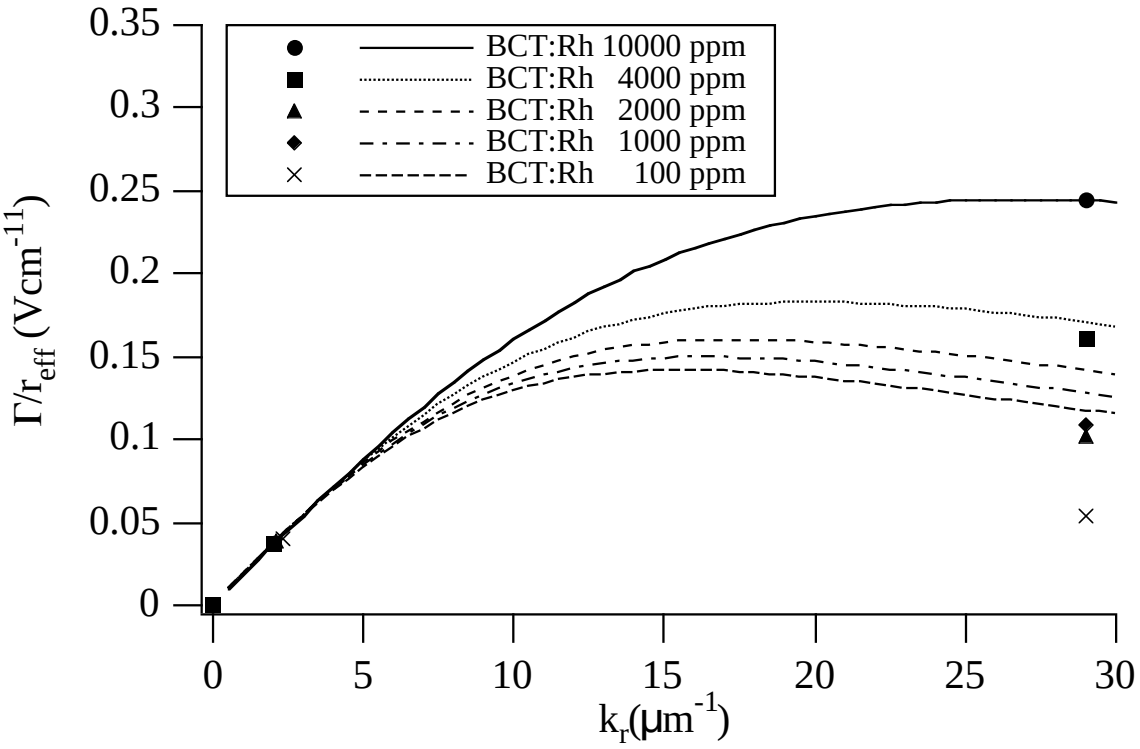

Figure 12 : A. Radoua et al.